Published in final edited form as:

Sci Transl Med. 2016 November 09; 8(364): 364ra153. doi:10.1126/scitranslmed.aag2306.

Local and transient gene expression primes the liver to resist cancer metastasis

Tyler J. Goodwin[1], **Yingqiu Zhou**[2], **Sara N. Musetti**[1], **Rihe Liu**[2,3,*], and **Leaf Huang**[1,*,†]

[1]Division of Pharmacoengineering and Molecular Pharmaceutics, Eshelman School of Pharmacy, University of North Carolina at Chapel Hill, Chapel Hill, NC 27599, USA

[2]Division of Chemical Biology and Medicinal Chemistry, Eshelman School of Pharmacy, University of North Carolina at Chapel Hill, Chapel Hill, NC 27599, USA

[3]Carolina Center for Genome Sciences, University of North Carolina at Chapel Hill, Chapel Hill, NC 27599, USA

Abstract

The liver is the primary site of metastasis for gastrointestinal cancers and is a location highly susceptible to the establishment of metastasis in numerous other primary cancers, including breast, lung, and pancreatic cancers. The current standard of care typically consists of primary tumor resection and systemic administration of potent but toxic chemotherapeutics, yielding a minimal improvement in the median survival rate. CXCL12, a chemokine, is a key factor for activating the migration/survival pathways of $CXCR4^+$ cancer cells and for recruiting immunosuppressive cells to areas of inflammation. Therefore, reducing CXCL12 concentrations within the liver has the potential to decrease tumor and immunosuppressive cell activation/migration within the liver. However, because of off-target toxicities associated with systemic administration of anti-CXCL12 therapies, transient and liver-specific expression of a CXCL12 trap is necessary. To address this challenge, we developed a lipid calcium phosphate nanoparticle optimized for delivering plasmid DNA, encoding an engineered CXCL12 protein trap, to the nucleus of liver hepatocytes. This pCXCL12-trap formulation yielded transient (4 days) liver-specific expression, which greatly decreased the occurrence of liver metastasis in two aggressive liver metastasis models, including colorectal [CT-26(FL3)] and breast (4T1) cancers. Subsequent studies in an aggressive human

*Corresponding author. leafh@email.unc.edu (L.H.); rliu@email.unc.edu (R.L.).
†Present address: Eshelman School of Pharmacy, University of North Carolina at Chapel Hill, 1315 Kerr Hall CB# 7571, Chapel Hill, NC 27599, USA.

SUPPLEMENTARY MATERIALS

www.sciencetranslationalmedicine.org/cgi/content/full/8/364/364ra153/DC1

Materials and Methods

Reference (28)

Author contributions: T.J.G., R.L., and L.H. conceived and designed the research. T.J.G. and Y.Z. performed the in vitro protein expression and characterization experiments. T.J.G. performed the in vivo mouse experiments. T.J.G. and S.N.M. prepared, analyzed, and quantified the histology. T.J.G. and S.N.M. performed the statistical analysis. T.J.G., R.L., and L.H. analyzed the data and wrote the manuscript.

Competing interests: U.S. Provisional Patent application no. 62/232,169 was filed on 24 September 2015 covering the LCP and pTrap technologies described.

Data and materials availability: All data for this study are presented here, and all material is available for noncommercial researchers via a materials transfer agreement.

colorectal liver metastasis model (HT-29) decreased the establishment of liver metastasis more effectively than did systemic administration of the CXCL12 protein trap and to a level comparable to a high-dose regimen of a potent CXCR4 antagonist (AMD3100).

INTRODUCTION

Colorectal cancer (CRC) is the third most prevalent cancer diagnosed worldwide and the third leading cause of cancer deaths. In the United States alone, about 143,460 patients were diagnosed, resulting in more than 51,690 deaths in 2012 (1). However, the cause of death is rarely due to the primary colon cancer burden itself, because local resection of cancerous colon is quite efficient. Unfortunately, the establishment of liver metastasis is the leading cause of death (1). At early stages of CRC detection, before liver metastases form, the 5-year survival rate is about 90%. Regrettably, this rate drops to less than 12% once liver metastasis has been established. By the time of diagnosis, 20% of patients have developed liver metastasis, and 60 to 70% of patients develop metastatic lesions in the liver by the time of death (2). Currently, the approved treatment for liver metastasis consists of liver resection and/or a combination of 5-fluorouracil with oxaliplatin or irinotecan with or without capecitabine. These treatments yield an overall response rate of 20 to 30% or 40 to 50%, depending on regimen, and a median overall survival of 12 to 20 months (3). Although these treatments are currently the standard of care and yield improved efficacy over other traditional treatments, the off-target toxicities along with a median survival of 12 to 20 months presents a less than desirable outcome. Therefore, a key strategy to improve the survival rate and quality of life for patients with CRC and other cancers undergoing treatment is to reduce off-target toxicities. This can be achieved through tissue-specific targeting of central factors that directly activate liver metastasis and subsequently promote the establishment of an immunosuppressive tumor microenvironment.

The relationship between the chemokine receptor CXCR4 expressed on cancer cells and its chemokine ligand, stromal derived factor-1 (CXCL12/SDF-1), secreted by the hepatic stellate cells (HSCs), plays a vital role in CRC and numerous other cancer liver metastasis (4). These HSCs are resident perisinusoidal cells that have been shown to produce high amounts of endogenous CXCL12 for recruitment of immunosuppressive lymphocytes such as regulatory T cells (T_{regs}) and myeloid-derived suppressor cells (MDSCs) to areas of inflammation. In the presence of high amounts of CXCL12, $CXCR4^+$ CRC cells migrate and invade along the CXCL12 concentration gradient. In addition, CXCR4 is expressed in a maintenance capacity in CRC progenitor cells to maintain stem-like characteristics (5, 6). Further analyses of human CRC biopsies have found that a higher rate of liver metastasis correlates with high expression of CXCR4 (4, 7). Therefore, we hypothesized that disrupting this CXCL12 gradient in the liver may effectively decrease the occurrence and progression of colorectal and numerous other $CXCR4^+$ cancers in the liver while drastically reducing the recruitment of immunosuppressive cells.

Treatment of mice with AMD3100 (plerixafor), a small-molecule CXCR4 antagonist, has demonstrated the therapeutic potential of disrupting the CXCL12/CXCR4 axis, resulting in the decreased occurrence of liver metastasis (8). Subsequently, many CXCR4 antagonists

have been developed (9). However, the endogenous role of CXCL12 and CXCR4 in the immune system is vital. These treatments, which include small-molecule and protein therapies, come with systemic off-target toxicity concerns. Furthermore, to our knowledge, no therapy targeted to CXCL12 has been developed and reported to reduce the occurrence of colorectal liver metastasis. Therefore, we hypothesized that an anticancer strategy centered on the liver-specific delivery of a gene encoding a small antibody-like protein to entrap CXCL12, and thereby alter the liver microenvironment, could be used to halt metastasis to the liver. Delivery of such genes can achieve reduced concentrations of CXCL12 or similar factors, priming the liver to directly reduce activation of the migration/invasion/survival/proliferation pathways in $CXCR4^+$ CRC cells. Furthermore, this strategy has the potential to decrease the recruitment of $CXCR4^+$ immunosuppressive cell types. Therefore, targeting protein factors, such as CXCL12, in the micro-environment of healthy tissue brings about an anticancer paradigm in which the metastatic lesions are not targeted directly. Instead, the metastasis-prone environment is primed to be unsuitable for the metastasis to form or progress, ultimately decreasing the establishment and growth of metastatic lesions.

The development and use of a reliable syngeneic orthotopic colorectal liver metastasis animal model enabled investigation into the role of CXCL12 in promoting liver metastasis. This model, first reported by Zhang *et al.*, involves inoculation of 2.0×10^6 CT-26(FL3) cells into the cecum wall to yield a high occurrence of liver metastasis (~90%) within 4 weeks (10). Subsequent establishment of a CT-26(FL3) cell line stably expressing red fluorescent protein (RFP)/luciferase (Luc) marker genes allowed the use of luciferase bioluminescent analysis to determine in vivo liver tumor burden. Through the use of this model, as well as the establishment of liver metastasis via hemi-splenic inoculation of human colorectal (HT-29) or mouse breast cancer (4T1) cell lines, we could investigate our therapy's ability to prime the liver microenvironment and the tumor/immune cell profile. The use of syngeneic models allowed us to investigate the immune profile and the role of cytotoxic T lymphocytes (CTLs) in reducing the progression and establishment of liver metastasis. Furthermore, investigation of liver metastasis in an immunodeficient athymic mouse model provides insight into whether the direct disruption of the CXCR4/CXCL12 axis on the cancer cells' surface is a therapeutic pathway for reducing the establishment of liver metastasis. These mouse models produce a reliable platform to examine whether the proposed strategy can be used to demonstrate in vivo anticancer efficacy on numerous $CXCR4^+$ derived colorectal cell lines, such as CT-26(FL3) and HT-29, as well as other cancers such as breast cancer (4T1) (fig. S1). We hypothesized that the targeted (liver-specific) delivery and transient expression of the engineered CXCL12 trap (Trap; 28.6 kDa) via a lipid calcium phosphate (LCP) nonviral vector can direct the liver to resist infiltrating $CXCR4^+$ metastatic cells as well as inhibit the establishment of an immunosuppressive tumor microenvironment, allowing for enhanced cancer-specific $CD8^+$ T cell killing.

RESULTS

Reduction of migration/invasion of CXCL12-stimulated CT-26(FL3) cells by engineered CXCL12 trap

The CXCL12 trap gene was designed on the basis of known anti-CXCL12 antibody sequences. This was accomplished by fusing a V_H and a V_L domain through a protease-resistant flexible linker. Subsequently, a strong signaling peptide from human serum albumin preproprotein was incorporated at the N terminus to efficiently facilitate the secretion from liver hepatocytes after expression (11), whereas E and His(6×) tags were introduced at the C terminus to facilitate protein purification and in vivo expression analysis. The coding sequence of the CXCL12 trap was cloned into the expression vector pCDNA3.1, driven by a cytomegalovirus promoter. The recombinant CXCL12 trap was expressed in and purified from 293 T cells. The target-binding features, such as the binding affinity and specificity for CXCL12 and other chemokines, were measured through biolayer interferometry (BLI) (Fig. 1A). The engineered CXCL12 trap was found to have a dissociation constant (K_d) of 4.1 nM for CXCL12 (Fig. 1A). It has been reported that treatment of CT-26(FL3) cells with the recombinant CXCL12 chemokine yields up-regulation of the migration/invasion pathways (4, 5). Therefore, we investigated the ability of our CXCL12 trap (Trap) and a commercially available CXCL12 antibody to suppress the migration and invasion of CT-26(FL3) cells down a concentration gradient of CXCL12 (Fig. 1, B and C). Although the in vitro half-maximal inhibition (ND_{50}) is not a direct indicator of affinity of the CXCL12 trap or CXCL12 antibody to the CXCL12, these in vitro experiments demonstrated the Trap's ability to decrease the migration and invasion of CT-26(FL3) (RFP/Luc) cells down a concentration gradient of CXCL12 (10 nM). Our results indicate complete suppression of the migration and invasion at a Trap concentration of 240 nM (Fig. 1, B and C). The CXCL12 trap produced ND_{50} against biologically active CXCL12 (10 nM) in vitro at a concentration of about 120 nM (Fig. 1, B and C). Commercially available CXCL12 antibody (ND_{50} of 12 to 24 nM) was used as a positive control (Fig. 1, B and C).

Formulation and characterization of galactose-LCP pDNA/mc-CR8C nanoparticles

Hu *et al.* (12) reported the formulation and delivery of the galactose-LCP with pDNA/mc-CR8C cargo to the liver hepatocytes of mice. The core structure can be visualized under transmission electron microscopy (TEM) (fig. S2A). The 1,2-dioleoyl-*sn*-glycero-3-phosphate (DOPA) monolayer surrounding the CaP core allows for the addition of the cationic outer leaflet lipids, 1,2-dioleoyl-3-trimethylammonium-propane (DOTAP), helper lipid cholesterol, and galactose conjugated to 1,2-distearoyl-*sn*-glycero-3-phosphatidylethanolamine-*N*-succinyl(polyethylene glycol)-2000 (GAL-DSPE-PEG2000) to assist in reticuloendothelial system, RES, evasion and hepatocyte uptake, producing the final LCP particles (40 to 60 nm in diameter, shown in fig. S2, B and C). The hydrodynamic diameter and the surface charge of the LCP particles were found via dynamic light scattering (DLS) zetasizer analysis to be about 45 nm and 10 mV, respectively (fig. S2C). The excess lipids not incorporated into the outer lipid layer of the LCP form liposomes with a diameter of about 350 nm. The LCP and liposome mixture result in a *z* average of 236 ± 32 nm (n = 6). The solution was found to be stable in 10% fetal bovine serum at 37°C for at least 24 hours in which no significant increase in the *z* average was observed (fig. S2D). The pDNA

encapsulation efficiency was found to be about 50 to 60%, which corresponds closely to the reported formulation by Hu *et al.* (12). Liver specificity, pharmaco-kinetics (PK), and organ distribution were determined through incorporation of ^{177}Lu radioisotope along with the nuclear-localizing signal peptide/pDNA into the LCP core. The LCP particles containing ^{177}Lu were injected through the tail vein into healthy BALB/c mice. The PK and organ distribution profile studies demonstrate that the galactose-LCP nanoparticles exhibit a two-phase distribution with $T_{1/2}$a and $T_{1/2}$b of 20 and 1054 min, respectively, as well as about 50% of the injected dose per gram tissue accumulating in the liver 16 hours after intravenous injection (fig. S3).

In vivo expression profile of pDNA (pGFP and pTrap) via LCP formulation

Hu *et al.* reported that most of the pDNA encapsulated in the highly PEGylated LCP vector was delivered and expressed in the hepa-tocytes. Furthermore, the decreased PEG density and the absence of a galactose-targeting ligand shifted the uptake preferentially into the Kupffer cells, decreasing expression of the pDNA (12). Therefore, to ensure hepatocyte uptake and expression, we used a high PEG density (30% mol input) and galactose-targeting ligand (5% mol input) throughout the formulation of the pDNA LCP vector. We investigated the preferential expression of the green fluorescent protein plasmid (pGFP) and CXCL12 trap plasmid (pTrap) in the liver versus other organs/serum to ensure preferential liver-specific expression of the delivered pDNA. We delivered pGFP LCP to observe GFP expression in the liver (Fig. 2A). Through fluorescent microscopy analysis of organ sections on days 2, 4, and 8 after the final pGFP LCP injection, we could demonstrate transient liver-specific expression lasting up to 4 days. No GFP signal was found in any other major organ sections. Furthermore, expression of GFP was found to be predominately in the hepatocyte population within the liver (fig. S4). Subsequently, expression of the CXCL12 trap was assessed by enzyme-linked immunosorbent assay (ELISA) and Western blot analysis using the His(6×)-tag engineered at the C terminus of the CXCL12 trap (Fig. 2, B and C). Mice were treated with increasing doses of pTrap LCP (0.1, 0.5, and 1.0 mg/kg). Through ELISA and Western blot analysis, we observed a dose-dependent increase in liver expression 24 hours after intravenous injection, with no significant expression found in other major organs or serum (Fig. 2B). Further, Western blot studies demonstrated the transient expression time profile in which pTrap LCP (10 mg of pDNA; 0.5 mg/kg every other day × 3) was administered intravenously followed by collection of the livers on days 1, 2, 4, and 8 after the final LCP administration (Fig. 2C). The results indicate that the pDNA LCP vector elicits transient liver-specific expression of the CXCL12 trap, similar to the GFP expression profile, yielding expression for at least 4 days after the final injection (10 mg of pDNA; 0.5 mg/kg every other day × 3) (Fig. 2, A to C). These results demonstrate that the galactose-LCP vector allows for preferential transient expression in the hepatocytes, with minimal expression in other organs or serum (Fig. 2).

Modifying CXCL12 expression and immune cell populations in the liver of CRC mice

Colorectal liver metastasis was established through injection of 2×10^6 CT-26(FL3) cells into the mouse cecum wall. Zhang *et al.* reported that initial micrometastatic lesions form 14 days after inoculation of cells. The formation of large metastatic lesions and euthanasia of the mice because of large primary tumors in the intestine was reported 4 weeks after

inoculation (10), which corresponded closely to our observations. Therefore, prophylactic liver metastasis treatment with pTrap LCP (10 mg of pDNA; 0.5 mg/kg every other day × 3) was initiated 10 days after inoculation, before the formation of measurable liver metastases. We first assessed whether the delivery of pTrap LCP would decrease CXCL12 concentrations as well as inflammation as a result of the reduced presence of metastatic lesions, as shown in Fig. 3A. The expression of endogenous CXCL12 in the liver of CRC-bearing BALB/c mice was investigated in liver sections through immunofluorescence staining for CXCL12. The amount of CXCL12 found in the livers of CRC mice was compared to sections obtained from normal (healthy) mice without CRC to better understand the shifts in the endogenous expression of CXCL12 in the CRC liver metastasis model. The livers were assessed on day 24 (10 days after the final injection) by staining for CXCL12 (red, Fig. 3A). We studied five groups, four of which contained CRC, as follows: healthy (no CRC), untreated [treated with phosphate-buffered saline (PBS)], pGFP LCP control (10 mg every other day × 3), pTrap LCP (10 mg, single injection), and pTrap LCP (10 mg every other day × 3). Figure 3A shows that the untreated and pGFP-treated CRC mice had comparable expression of CXCL12 and that it was five- to sixfold higher than in the healthy livers from mice without CRC. The increased CXCL12 is believed to be a result of inflammation induced by the presence of the metastatic lesions. However, pTrap LCP (10 mg and 10 mg every other day × 3) treatment resulted in 2.5- and 5-fold decreases in fluorescence intensity, respectively, compared to the untreated animals, reaching baseline expression of CXCL12 in the group that received three doses of the Trap (Fig. 3A). Endogenous expression of CXCL12 in major organs of healthy mice (no CRC) is shown in fig. S5. Having observed the reduction in liver CXCL12 after treatment with pTrap LCP, we further stained the tissue sections to determine the effect of treatment on the liver immune cell populations, including MDSCs, T_{regs}, and $CD8^+$ T cells (Fig. 3B). These immune cells have substantial CXCR4 expression and therefore are recruited by endogenous CXCL12 (13). Four groups were studied, including sections from the livers of healthy mice (no CRC), untreated livers containing metastatic lesions (tumor), untreated livers containing increased collagen (stroma), as well as those treated with pTrap LCP (10 mg every other day × 3), in which metastatic lesions were not observed. The staining indicated that there is a drastic increase in the MDSC, T_{reg}, and $CD8^+$ T cell population in the untreated (tumor and stroma) groups compared to the healthy (no CRC) group. The pTrap LCP–treated group had low numbers of MDSCs and T_{regs}, similar to the healthy livers (no CRC). However, an increase was observed in the $CD8^+$ T cell population in the pTrap LCP group compared to the healthy (no CRC) group. It must be noted, however, that this amount of $CD8^+$ T cells was still twofold lower than in the untreated groups, in which metastatic lesions and inflammation were present (Fig. 3B). This is consistent with the metastatic lesions' ability to cause local inflammation, which results in increased CXCL12 and a subsequent influx of anti- and proinflammatory immune cells into the liver (Fig. 3B). Although the untreated CRC livers had the highest influx of $CD8^+$ T cells, the large numbers of immunosuppressive MDSC and T_{reg} populations are likely to neutralize the $CD8^+$ T cells before they can mediate cancer-specific killing. However, after pTrap treatment, the moderate increase in the $CD8^+$ T cell population in the presence of minimal immunosuppressive cells may allow for adequate surveillance and cancer-specific killing before the immunosuppressive metastatic lesion is formed.

Therapeutic efficacy of pTrap LCP in an orthotopic syngeneic colorectal liver metastasis mouse model

We examined the effect of pTrap LCP on the incidence of liver metastasis in mice. Mice were inoculated with 2.0×10^6 CT-26(FL3) (RFP/Luc) cells orthotopically into the cecum wall. Three treatment groups were evaluated, including untreated (PBS), a vector/pDNA control (pGFP LCP), and pTrap LCP. Administration of treatment began on day 10 after inoculation. Intravenous tail vein injections [10 mg (0.5 mg/kg) of pDNA] were administered on days 10, 12, and 14. The total tumor burden was monitored by intraperitoneal administration of 200 ml of luciferin (10 mg/ml) followed by bio-luminescent analysis 10 min after luciferin administration. The tumor burden was recorded weekly and used to sort mice into treatment groups before day 10. The tumor burden on day 24 is shown in fig. S6. On day 24, mice were imaged and euthanized because of heavy primary tumor burden in the cecum. Livers and other organs were harvested and analyzed by bioluminescence imaging to determine metastatic tumor burden (Fig. 4, A and B). After bioluminescent analysis, livers were fixed, sectioned, and trichrome-stained for further morphological analysis (Fig. 4C). Mice treated with PBS or pGFP LCP developed large metastatic tumor lesions in the liver (Fig. 4, A and B), which caused prominent fibrotic tissue and cirrhosis (Fig. 4C). In contrast, mice treated with pTrap LCP (10 mg of pDNA) three times showed a 10-fold reduction in liver metastasis burden and about a 70 to 80% decrease in the incidence of liver metastasis formation (Fig. 4, A and B). The fibrotic area detected by microscopic analysis of the trichrome-stained liver sections was significantly less in specimens from pTrap LCP mice than in control specimens ($P = 0.0001$) (Fig. 4C). Although the rate of liver metastasis was reduced, the primary and distal tumor burden outside of the liver remained unchanged with this treatment (Fig. 4B).

Enhancement of antimetastasis efficacy of pTrap LCP therapy by cancer-specific T cells

The decreased MDSC and T_{reg} populations in the liver after pTrap LCP treatment, along with the presence of $CD8^+$ lymphocytes, implicate a shift from a protumor (immunosuppressive) to antitumor environment within the liver. Therefore, we examined the CTLs' ability to decrease the establishment of metastasis in the liver after pTrap LCP therapy. To investigate the pTrap LCPs' ability to enhance cancer-specific $CD8^+$ T cell killing, we studied the anticancer efficacy of the pTrap LCP in mice with a depleted $CD8^+$ T cell population. We followed a protocol similar to that reported by Harimoto *et al.* (14), in which ≥95% of the $CD8^+$ T cell population was depleted after two intraperitoneal injections of 400 mg of anti-Lyt2.2 [2.43; rat immunoglobulin G2b (IgG2b)]. Mice were inoculated with CRC according to the orthotopic syngeneic model described earlier, followed by T cell depletion before treatment. In this series of experiments, the animals were divided into three treatment groups: untreated (PBS), pTrap LCP with anti-CD8 (anti-Lyt2.2), and pTrap LCP with an antibody isotype control (rat IgG2b isotype control). To maintain the depletion of the $CD8^+$ T cell population, we administered an intraperitoneal injection of the anti-Lyt2.2 or isotype control IgG (400 mg) on days 8 and 10. Treatment was initiated on day 10 after inoculation, with intravenous tail vein injection (10 mg of pDNA) on days 10, 12, and 14. Mice were euthanized because of heavy primary tumor burden in the cecum on day 21, and the liver tumor burden was determined through bioluminescence imaging (Fig. 5). All mice treated with the PBS developed large metastatic tumor lesions in the liver (Fig. 5). The T

cell– depleted mice treated with anti-Lyt2.2 followed by three doses of pTrap LCP (10 mg of pDNA) showed similar liver tumor burden to the untreated mice. In contrast, mice treated with the isotype control IgG2b antibody followed by pTrap LCP showed a fivefold reduction in liver metastasis burden and about an 80% decrease in the incidence of liver metastasis compared to untreated animals. These results show that the presence of CTLs, along with reduction in CXCL12, decreases the risk of establishing metastatic lesions in the liver.

Reduced metastatic burden and increased survival in breast cancer liver metastasis model

We examined the effect of pTrap LCP on the median survival and liver tumor burden in an aggressive mouse breast cancer liver metastasis model. The breast cancer liver metastasis model consists of the hemi-splenic implantation of a highly metastatic murine breast cancer cell line 4T1. These studies modeled the clinical standard of care, in which the primary tumor is resected and death usually results from the metastatic burden. BALB/c mice were inoculated with 1.0×10^6 (0.1 ml) of 4T1(GFP/Luc) cells into one-half of the spleen, which had been tied off and separated into two halves before the tumor inoculation. The hemi-spleen that received the cells was resected 10 min after inoculation to decrease primary tumor growth. In this series of experiments, treatments began on the day of inoculation because of the rapid migration of cells to the liver, often within 5 min after inoculation (15). We studied four treatment groups for the breast cancer liver metastasis model: untreated (PBS), pGFP LCP with anti-CD8 [10 mg (0.5 mg/kg) of pDNA and 400 mg (20 mg/kg) of anti-Lyt2.2], pTrap LCP with anti-CD8 [10 mg (0.5 mg/kg) of pDNA and 400 mg (20 mg/kg) of anti-Lyt2.2], and pTrap LCP with isotype IgG [10 mg (0.5 mg/kg) of pDNA and 400 mg (20 mg/kg) of isotype IgG]. PBS, pGFP LCP, or pTrap LCP was administered intravenously via tail vein injections every other day starting on day 0 and ending on day 6. Administration of the anti-Lyt2.2 or isotype IgG control involved two intraperitoneal injections on days 0 and 2. Tumor progression was monitored by bioluminescence imaging (Fig. 6A). Mice were euthanized when one of the following conditions applied: drastic weight gain or loss greater than 10% within 1 week or clear signs of distress, such as dehydration, inactivity, or shortness of breath/weak breathing. Three mice from each group were euthanized 10 days after inoculation, their organs were collected and rinsed in PBS, and the livers were analyzed for tumor burden by flow cytometry analysis (Fig. 6B). Mice that did not receive pTrap LCP treatment developed large metastatic tumor lesions in the liver within the first week after inoculation (Fig. 6, A and B). In contrast, mice treated with pTrap LCP showed a reduction in liver metastasis burden and decrease in the incidence of liver metastasis formation, as well as an almost twofold increase in the median survival versus all other treatment groups (14 days versus 25 days) (Fig. 6C).

Reducing the establishment of liver metastasis by pTrap LCP, Trap protein, and CXCR4 antagonist

We compared the efficacy of different therapeutic modalities [anti-CXCL12 trap protein, CXCR4 small-molecule antagonist (AMD3100), and the pTrap LCP] in reducing the establishment of liver metastasis using a human CRC cell line (HT-29) in immunodeficient athymic mice. The human CRC liver metastasis model was established according to the same hemi-splenic implantation procedure as above, using CRC cell line HT-29, which has high expression of CXCR4 (fig. S1). In this series of experiments, treatments again began on

the day of inoculation because of the rapid migration of cells to the liver within 5 min after inoculation (15). The five treatment groups studied for the CRC liver metastasis model were untreated (PBS), pGFP LCP [10 mg (0.5 mg/kg) of pDNA], pTrap LCP [10 mg (0.5 mg/kg) of pDNA], free CXCL12 trap protein [10 mg (0.5 mg/kg) of protein], and AMD3100 (100 mg, 5.0 mg/kg). The treatments were administered intravenously by tail vein injection every other day, initiated on day 0, and terminated on day 16 (Fig. 7A). Mice were euthanized on day 36, their livers were collected and rinsed in PBS, and tumor nodules were resected from the livers and weighed (Fig. 7B). Mice that did not receive pTrap LCP or AMD3100 treatment developed numerous metastatic tumor lesions in the liver (Fig. 7B). In contrast, mice treated with pTrap LCP or AMD3100 showed a reduction in liver metastasis burden and decreased incidence of liver metastasis formation compared to all other treatment groups.

Toxicity analysis of pTrap LCP and free CXCL12 trap protein

Administration of pTrap LCP (10 mg every other day × 3) did not cause any significant changes in alanine aminotransferase (ALT), aspartate aminotransferase (AST), creatinine, or blood urea nitrogen (BUN), and there were no signs of toxicity in trichrome-stained histology sections of any organ 24 hours after the final intravenous tail vein injection (Fig. 8, A and B). Analysis of blood cell counts showed no signs of change compared to untreated mice (Fig. 8A). However, analysis of mouse serum and whole blood samples after systemic intravenous injection of 20 mg of engineered CXCL12 trap protein (every other day × 3) identified transient elevations of ALT and AST on day 7 after the final injection. In addition, the white blood cell counts drastically decreased between days 1 and 7, with a slight recovery of white blood cell counts by day 14 after the final injection (Fig. 8A). Histological analysis of trichrome-stained organ sections found no signs of toxicity for any of the treatment groups.

DISCUSSION

To prime the liver to resist cancer invasion, we must block the factor(s) that plays a pivotal role in cancer progression. Our decision to target CXCL12 stemmed from numerous studies demonstrating the fundamental role that CXCL12 plays in up-regulating cancer pathways and recruiting immunosuppressive cell types to the tumor microenvironment. CXCR4 is the most widely expressed chemokine receptor, with high expression in many different hematological and solid cancers (16). High expression of CXCR4 is associated with high rates of liver metastasis and poor survival (4). CXCR4 is activated by the exclusive binding of its ligand CXCL12. CXCL12 activates essential signaling pathways, including epidermal growth factor receptor, mitogen-activated protein kinase (MAPK), phosphoinositide 3-kinase/protein kinase B (PI3K/AKT), WNT, and nuclear factor kB (NF-kB), which mediate cancer cell proliferation, growth, migration, invasion, and survival (17). Recent studies suggest that the stimulation of tumor cell proliferation via CXCL12 is MAPK-dependent (18, 19). This CXCL12 stimulation can further be categorized as an autocrine mechanism, in which CXCL12 activates RAS and MAPK, allowing for the production of various transcription factors including c-MYC. These transcription factors further up-regulate the expression of CXCR4, resulting in enhanced sensitivity to CXCL12 (17, 20). Another study

found that inhibition of CXCL12/CXCR4 signaling decreased pancreatic cancer proliferation and progression in vitro via inactivation of the canonical WNT pathway (21). In addition, CXCL12 influences tumor growth through activation of the PI3K/AKT pathway (18, 19). The ability of CXCL12 to drive tumor cell survival was also established in a study suggesting that CXCL12 expression activates NF-kB and suppresses apoptotic signaling (22).

The progression of cancer from the primary lesion to distant metastatic lesions is the product of a highly organized and tissue-selective process. One such mechanism involves CXCL12 directing metastasis to select tissues through the establishment of a chemokine gradient. The CXCL12 chemokine can interact with glycosaminoglycan on the surface of endothelial cells and in the extracellular matrix to produce a concentration gradient. This chemokine gradient directs leukocyte and tumor cell migration toward a select tissue. In addition, CXCR4 is expressed in CRC progenitor cells and plays a role in maintaining these cancer stem-like cells (5, 6). Human breast cancer is another such example, where CXCR4 is highly expressed and stimulated by CXCL12 in both primary and metastatic lesions. CXCL12 is highly expressed in organs to which breast cancer disseminates, such as lung, bone, and liver. In vivo studies have demonstrated that neutralization of the CXCL12/CXCR4 axis impairs metastasis resulting from chemotactic and invasive responses in breast cancer models (23). CXCR4 is also involved in the metastasis of prostate cancer cells to the bone marrow, where a higher population of $CXCR4^+$ cells are found at the metastatic sites compared to the primary tumor (24, 25).

The research presented in this report demonstrates the therapeutic benefits of inhibiting CXCL12 in the liver of aggressive liver metastasis cancer models. Directly disrupting the activation of $CXCR4^+$ cancer cells by inhibiting CXCL12 in an immunodeficient CRC liver metastasis mouse model reduced the establishment of liver metastasis. Furthermore, in immunocompetent colorectal and breast cancer liver metastasis mouse models, we demonstrated that disrupting the CXCL12/CXCR4 pathway also plays a crucial role in inhibiting the tumor immunosuppresive microenvironment. CXCL12/CXCR4 plays a critical role in the recruitment of leukocytes, plasmacytoid dendritic cells, MDSCs, and neutrophils to sites of inflammation (13). Studies have suggested that increasing amounts of CXCL12 are produced by the HSCs during liver inflammation. This local increase in CXCL12 production drives recruitment and activation of tumor and immune cells to the microenvironment. These infiltrating cells provide an additional source of CXCL12 at the inflammation site (metastatic lesion), which further activates tumor growth, survival, angiogenesis, and metastasis. Our results suggest that delivery of a CXCL12 trap to the liver not only disrupts cancer activation by inhibiting CXCL12/CXCR4 interaction but also inhibits the recruitment of $CXCR4^+$ immunosuppressive cells such as MDSCs and T_{regs}. Therefore, we hypothesize that our therapy works by two major pathways, directly inhibiting the CXCL12/CXCR4 stimulation of cancer cells and reducing the recruitment of $CXCR4^+$ immunosuppresive cells to allow for increased cancer-specific $CD8^+$ T cell killing. The local (liver) and transient (4 days) expression of the engineered CXCL12 trap has the potential to influence the immune response and the cancer biology driving the establishment of metastasis. These findings may provide a basis for future strategies for targeting metastatic

lesions, in which the co-delivery of genes expressing traps against a chemokine such as CXCL12 and an immune checkpoint protein could work in a synergistic manner.

Clinically, it has been suggested that the number of $CXCR4^+$ CRC cells in a patient can be used as a biomarker to determine which patients may have a more aggressive and higher rate of liver metastasis (4, 7). Therefore, patients with a large population of $CXCR4^+$ cells may be optimal candidates for a treatment targeting the CXCL12/CXCR4 axis in conjunction with other therapies. However, it is also clear that endogenous CXCL12 plays a crucial role in leukocyte recruitment, and therefore, systemic administration of free anti-CXCL12 proteins would elicit serious toxicities. We demonstrate that these toxicities can be avoided through the local and transient delivery of LCP gene vector. This pTrap LCP vector enabled us to greatly decrease the occurrence of colorectal liver metastasis (80%) and drastically decrease the tumor burden found within the liver (10-fold). Increased concentrations of the CXCL12 trap and decreased concentrations of free CXCL12 protein were found in the liver in a dose-dependent manner. This approach also reduced the recruitment of immune suppressor cells (MDSCs and T_{regs}), demonstrating a biologically specific effect of pTrap LCP treatment. The insufficient target specificity of most small-molecule and protein therapies as well as the toxicity concerns that revolve around the use of viral vectors for gene therapy have limited the clinical applications. Furthermore, many nonviral vectors for gene therapy have fallen short because of extracellular and intracellular barriers in vivo. However, the delivery of pDNA in an LCP vector shows no signs of off-target effects, with minimal to no adverse immune response after repeated injections. The ability to have transient expression of this small CXCL12 trap (~28.6 kDa) (fig. S7) lasting up to about 4 days would allow clinicians to tightly control and monitor the extent and time of expression to limit undesired immune responses and still achieve therapeutic efficacy. Moreover, the in vivo pDNA dose used in our study (0.5 mg/kg per injection) is substantially lower than doses previously shown to have in vivo expression (26). In the past, therapeutic pDNA has only been successfully delivered to the liver via viral vectors or through invasive hydrodynamic injection (27). Therefore, a nonviral vector capable of delivering a therapeutic gene, such as the CXCL12 trap, should have high translatability to the clinic.

Although this LCP platform and many other nonviral vectors have aimed to improve pDNA expression in vivo, the expression of nonviral vectors still falls short compared to viral gene delivery systems. This gap can only be lessened through innovative technologies aimed at improving the limitations in nuclear localization and release of pDNA. Furthermore, the preclinical animal models used to test a vector's therapeutic potential need to more accurately mirror the clinical profile. The use of cell line–based models and nonorthotopic implantation introduce artifacts that limit our capacity to measure the nonviral vector's ability to treat clinical disease. These limitations will need to be addressed to bring about successful translation of these gene delivery vectors to the clinic.

MATERIALS AND METHODS

For detailed Materials and Methods, please see the Supplementary Materials.

Supplementary Material

Refer to Web version on PubMed Central for supplementary material.

Acknowledgments

This study was inspired by Debbie Whitmore, who succumbed to colorectal cancer liver metastasis. We thank M. M. O. Peña for providing the highly metastatic CT-26(FL3) cell line. We thank the histology core for help with the paraffin-embedded sections and trichrome stains, as well as the small animal imaging core at the University of North Carolina at Chapel Hill for help with training on the IVIS bioluminescence imaging.

Funding: This work was supported by NIH grants DK100664, CA151652, CA149387 (to L.H.), and CA157738, CA151652 (to R.L.) as well as an Eshelman Institute for Innovation grant (to L.H. and R.L.).

REFERENCES AND NOTES

1. American Cancer Society. Cancer Facts and Figures 2012. American Cancer Society Inc.; 2012. p. 25-26.
2. Schima W, Kulinna C, Langenberger H, Ba-Ssalamah A. Liver metastases of colorectal cancer: US, CT or MR? Cancer Imaging. 2005; 5:S149–S156. [PubMed: 16361131]
3. Ismaili N. Treatment of colorectal liver metastases. World J Surg Oncol. 2011; 9:154. [PubMed: 22115124]
4. Zeelenberg IS, Stalle L Ruuls-Van, Roos E. The chemokine receptor CXCR4 is required for outgrowth of colon carcinoma micrometastases. Cancer Res. 2003; 63:3833–3839. [PubMed: 12839981]
5. Kucia M, Reca R, Miekus K, Wanzeck J, Wojakowski W, Janowska-Wieczorek A, Ratajczak J, Ratajczak MZ. Trafficking of normal stem cells and metastasis of cancer stem cells involve similar mechanisms: Pivotal role of the SDF-1-CXCR4 axis. Stem Cells. 2005; 23:879–894. [PubMed: 15888687]
6. Lombardi L, Tavano F, Morelli F, Latiano TP, Di Sebastiano P, Maiello E. Chemokine receptor CXCR4: Role in gastrointestinal cancer. Crit Rev Oncol Hematol. 2013; 88:696–705. [PubMed: 24120239]
7. Zhang, S-s, Han, Z-p, Jing, Y-y, Tao, S-f, Li, T-j, Wang, H., Wang, Y., Li, R., Yang, Y., Zhao, X., Xu, X-d, Yu, E-d, Rui, Y-c, Liu, H-j, Zhang, L., Wei, L-x. $CD133^{+}CXCR4^{+}$ colon cancer cells exhibit metastatic potential and predict poor prognosis of patients. BMC Med. 2012; 10:85. [PubMed: 22871210]
8. Matsusue R, Kubo H, Hisamori S, Okoshi K, Takagi H, Hida K, Nakano K, Itami A, Kawada K, Nagayama S, Sakai Y. Hepatic stellate cells promote liver metastasis of colon cancer cells by the action of SDF-1/CXCR4 axis. Ann Surg Oncol. 2009; 16:2645–2653. [PubMed: 19588204]
9. Debnath B, Xu S, Grande F, Garofalo A, Neamati N. Small molecule inhibitors of CXCR4. Theranostics. 2013; 3:47–75. [PubMed: 23382786]
10. Zhang Y, Davis C, Ryan J, Janney C, Peña MM. Development and characterization of a reliable mouse model of colorectal cancer metastasis to the liver. Clin Exp Metastasis. 2013; 30:903–918. [PubMed: 23748471]
11. Kober L, Zehe C, Bode J. Optimized signal peptides for the development of high expressing CHO cell lines. Biotechnol Bioeng. 2013; 110:1164–1173. [PubMed: 23124363]
12. Hu Y, Haynes MT, Wang Y, Liu F, Huang L. A highly efficient synthetic vector: Nonhydrodynamic delivery of DNA to hepatocyte nuclei in vivo. ACS Nano. 2013; 7:5376–5384. [PubMed: 23647441]
13. Lazennec G, Richmond A. Chemokines and chemokine receptors: New insights into cancer-related inflammation. Trends Mol Med. 2010; 16:133–144. [PubMed: 20163989]
14. Harimoto H, Shimizu M, Nakagawa Y, Nakatsuka K, Wakabayashi A, Sakamoto C, Takahashi H. Inactivation of tumor-specific $CD8^{+}$ CTLs by tumor-infiltrating tolerogenic dendritic cells. Immunol Cell Biol. 2013; 91:545–555. [PubMed: 24018532]

15. Giavazzi R, Jessup JM, Campbell DE, Walker SM, Fidler IJ. Experimental nude mouse model of human colorectal cancer liver metastases. J Natl Cancer Inst. 1986; 77:1303–1308. [PubMed: 3467119]

16. Zlotnik A. Chemokines and cancer. Int J Cancer. 2006; 119:2026–2029. [PubMed: 16671092]

17. Thomas RM, Kim J, Revelo-Penafiel MP, Angel R, Dawson DW, Lowy AM. The chemokine receptor CXCR4 is expressed in pancreatic intraepithelial neoplasia. Gut. 2008; 57:1555–1560. [PubMed: 18664506]

18. Barbero S, Bonavia R, Bajetto A, Porcile C, Pirani P, Ravetti JL, Zona GL, Spaziante R, Florio T, Schettini G. Stromal cell-derived factor 1alpha stimulates human glioblastoma cell growth through the activation of both extracellular signal-regulated kinases 1/2 and Akt. Cancer Res. 2003; 63:1969–1974. [PubMed: 12702590]

19. Wu M, Chen Q, Li D, Li X, Li X, Huang C, TAng Y, Zhou Y, Wang D, Tang K, Cao L, Shen S, Li G. LRRC4 inhibits human glioblastoma cells proliferation, invasion, and proMMP-2 activation by reducing SDF-1 a/CXCR4-mediated ERK1/2 and Akt signaling pathways. J Cell Biochem. 2008; 103:245–255. [PubMed: 17549698]

20. Heinrich EL, Lee W, Lu J, Lowy AM, Kim J. Chemokine CXCL12 activates dual CXCR4 and CXCR7-mediated signaling pathways in pancreatic cancer cells. J Transl Med. 2012; 10:68. [PubMed: 22472349]

21. Wang Z, Ma Q, Liu Q, Yu H, Zhao L, Shen S, Yao J. Blockade of SDF-1/CXCR4 signalling inhibits pancreatic cancer progression in vitro via inactivation of canonical Wnt pathway. Br J Cancer. 2008; 99:1695–1703. [PubMed: 19002187]

22. Ganju RK, Brubaker SA, Meyer J, Dutt P, Yang Y, Qin S, Newman W, Groopman JE. The a-chemokine, stromal cell-derived factor-1a, binds to the transmembrane G-protein-coupled CXCR-4 receptor and activates multiple signal transduction pathways. J Biol Chem. 1998; 273:23169–23175. [PubMed: 9722546]

23. Luker KE, Luker GD. Functions of CXCL12 and CXCR4 in breast cancer. Cancer Lett. 2006; 238:30–41. [PubMed: 16046252]

24. Wang J, Wang J, Sun Y, Song W, Nor JE, Wang CY, Taichman RS. Diverse signaling pathways through the SDF-1/CXCR4 chemokine axis in prostate cancer cell lines leads to altered patterns of cytokine secretion and angiogenesis. Cell Signal. 2005; 17:1578–1592. [PubMed: 16005185]

25. Schimanski CC, Schwald S, Simiantonaki N, Jayasinghe C, Gönner U, Wilsberg V, Junginger T, Berger MR, Galle PR, Moehler M. Effect of chemokine receptors CXCR4 and CCR7 on the metastatic behavior of human colorectal cancer. Clin Cancer Res. 2005; 11:1743–1750. [PubMed: 15755995]

26. Goodwin T, Huang L. Nonviral vectors: We have come a long way. Adv Genet. 2014; 88:1–12. [PubMed: 25409601]

27. Song YK, Liu F, Zhang G, Liu D. Hydrodynamics-based transfection: Simple and efficient method for introducing and expressing transgenes in animals by intravenous injection of DNA. Methods Enzymol. 2002; 346:92–105. [PubMed: 11883099]

28. Kasuya H, Kuruppu DK, Donahue JM, Choi EW, Kawasaki H, Tanabe KK. Mouse models of subcutaneous spleen reservoir for multiple portal venous injections to treat liver malignancies. Cancer Res. 2005; 65:3823–3827. [PubMed: 15867380]

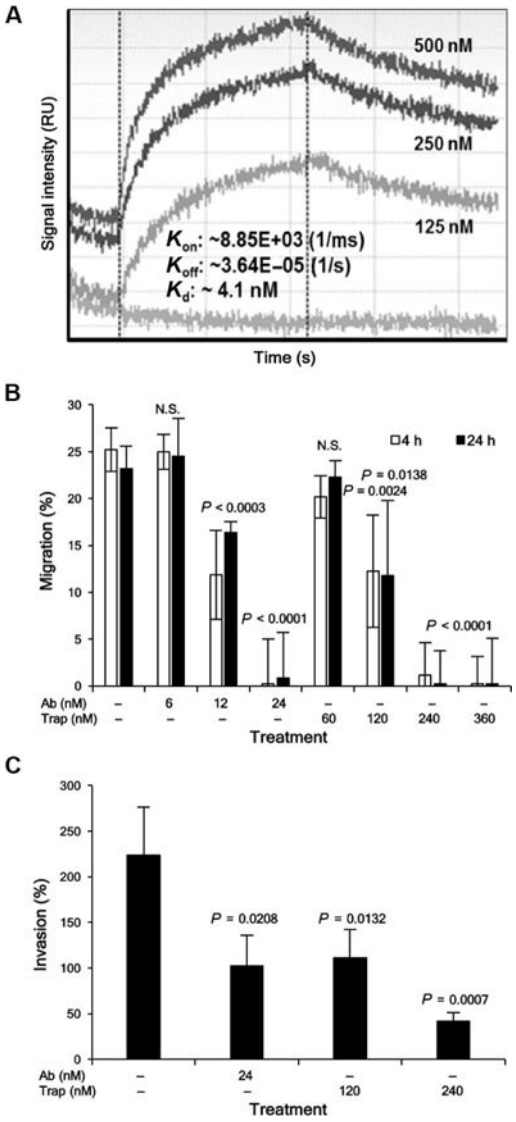

Fig. 1. Binding affinity and effect of engineered CXCL12 trap protein on in vitro cellular migration and invasion

(**A**) Binding affinity between CXCL12 trap and CXCL12 measured by BLI, where CXCL12 was immobilized on the AR2G biosensor and the binding kinetics were measured against no CXCL12 trap (0 nM) and increasing concentrations of CXCL12 trap (125, 250, and 500 nM) to determine the k_{on} and k_{off} rates depicted by the tracing of signal intensities versus time. The K_d was calculated to be 4.1 ± 0.4 nM after determining the on and off rate depicted. RU, resonance units. (**B**) The Chemotaxis Migration Assay Kit (EMD Millipore) with a pore size of 8 μm was used to investigate inhibition of cellular migration. We analyzed CT-26(FL3) cell migration toward a concentration gradient of CXCL12 (10 nM) in the presence of CXCL12 trap (60, 120, 240, or 360 nM). A positive control CXCL12 antibody (6, 12, or 24 nM) was also used. The engineered CXCL12 trap was found to have one-half maximal inhibition (ND_{50}) against biologically active CXCL12 (10 nM) at a concentration of 120 nM. (**C**) Invasion Assay Kit (EMD Millipore) with a pore size of 8 μm and ECMatrix were used to analyze the increase in CT-26(FL3) cell invasion toward a

concentration gradient of CXCL12 (10 nM) in the presence or absence of CXCL12 trap (120 or 240 nM) or control CXCL12 antibody (24 nM). Data are means ± SD, calculated from samples performed in triplicate and as a percentage of untreated (no CXCL12 or treatment protein) control. Cell migration and invasion were determined through cell collection, lysis, and quantification by luciferase bio-luminescent analysis. Statistical significance is indicated in graph compared to the control containing CXCL12 (10 nM) in the feeder (lower) plate without CXCL12 trap or antibody. N.S., not significant.

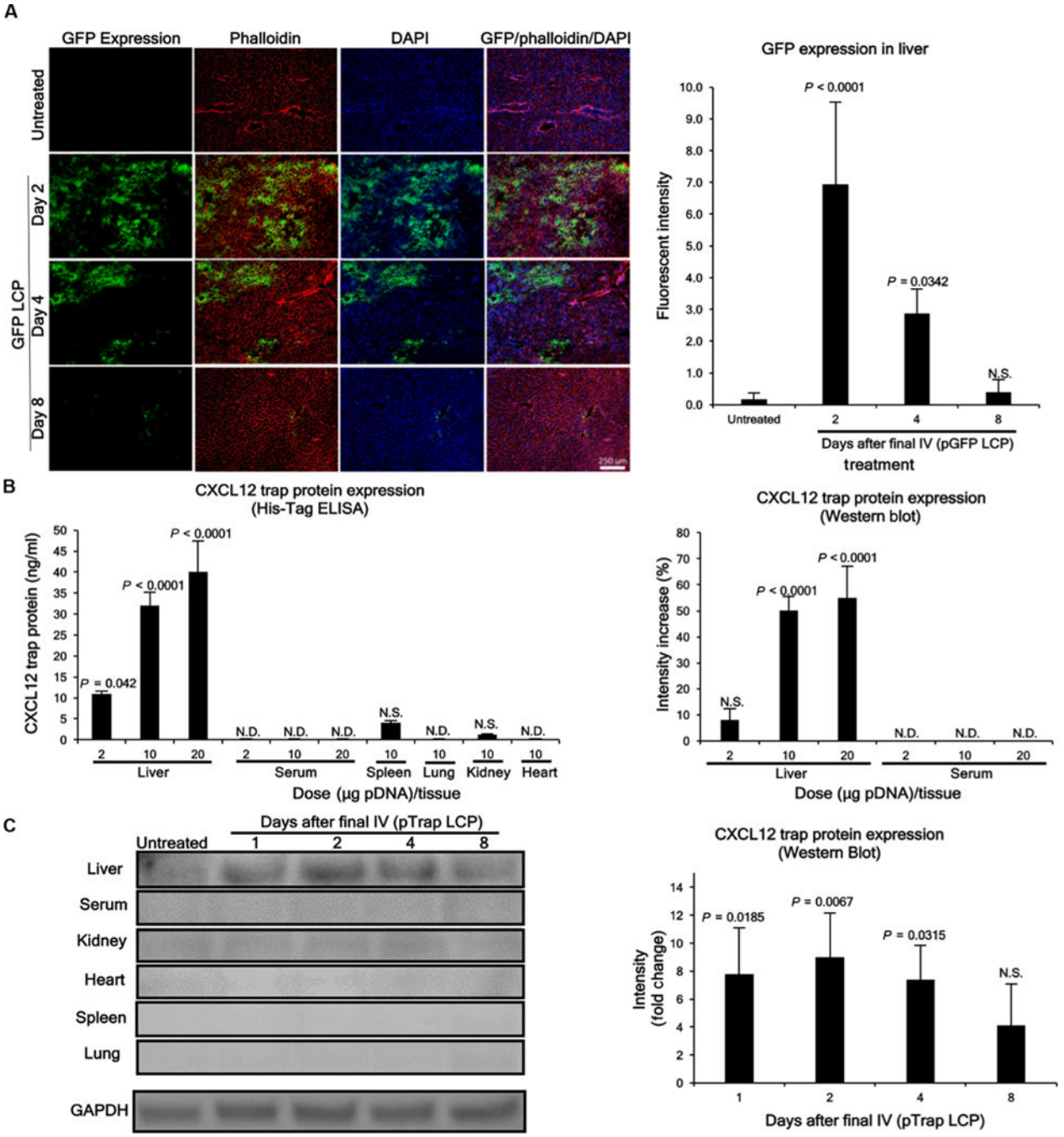

Fig. 2. Transient liver-specific expression of pGFP and engineered pTrap

(**A**) Microscopy analysis of GFP expression in major LCP-accumulating organs. The liver sections demonstrate transient expression for at least 4 days after the final injection (10 mg every other day × 3). Scale bar, 250 μm. Data are means ± SD, calculated from at least triplicated samples and reported as fluorescence intensity quantified by ImageJ software. N.D., under detection limit; *P* values represent significance of the difference from untreated sample. Scale bar, 250 μm. DAPI, 4′,6-diamidino-2-phenylindole; IV, intravenous. (**B**) His(6×)-tag ELISA and Western blot analysis were conducted to determine the organ

distribution/expression of the pTrap in all major LCP-accumulating organs and serum. Doses were escalated from 2.0 to 10.0 and 20.0 mg of pDNA administered via tail vein. (**C**) Western blot analysis of organs shows CXCL12 trap expression using His(6×) monoclonal antibody. The expression is transient and only lasts for 4 to 8 days after the final injection (10 mg every other day × 3). Total protein concentrations were determined by bicinchoninic acid assay, BCA, and 50 mg of total protein was loaded per well/lane. Trap protein was detected at 28.6 kDa, as confirmed by a protein standard ladder, consistent with the theoretical value. Glyceraldehyde-3-phosphate dehydrogenase (GAPDH) was used as a loading control, except in the serum samples, where GAPDH is not present. Data are means ± SD, calculated from samples run in triplicate and shown as a fold increase compared to untreated control. The *P* values of groups compared to corresponding untreated control are displayed in graphs.

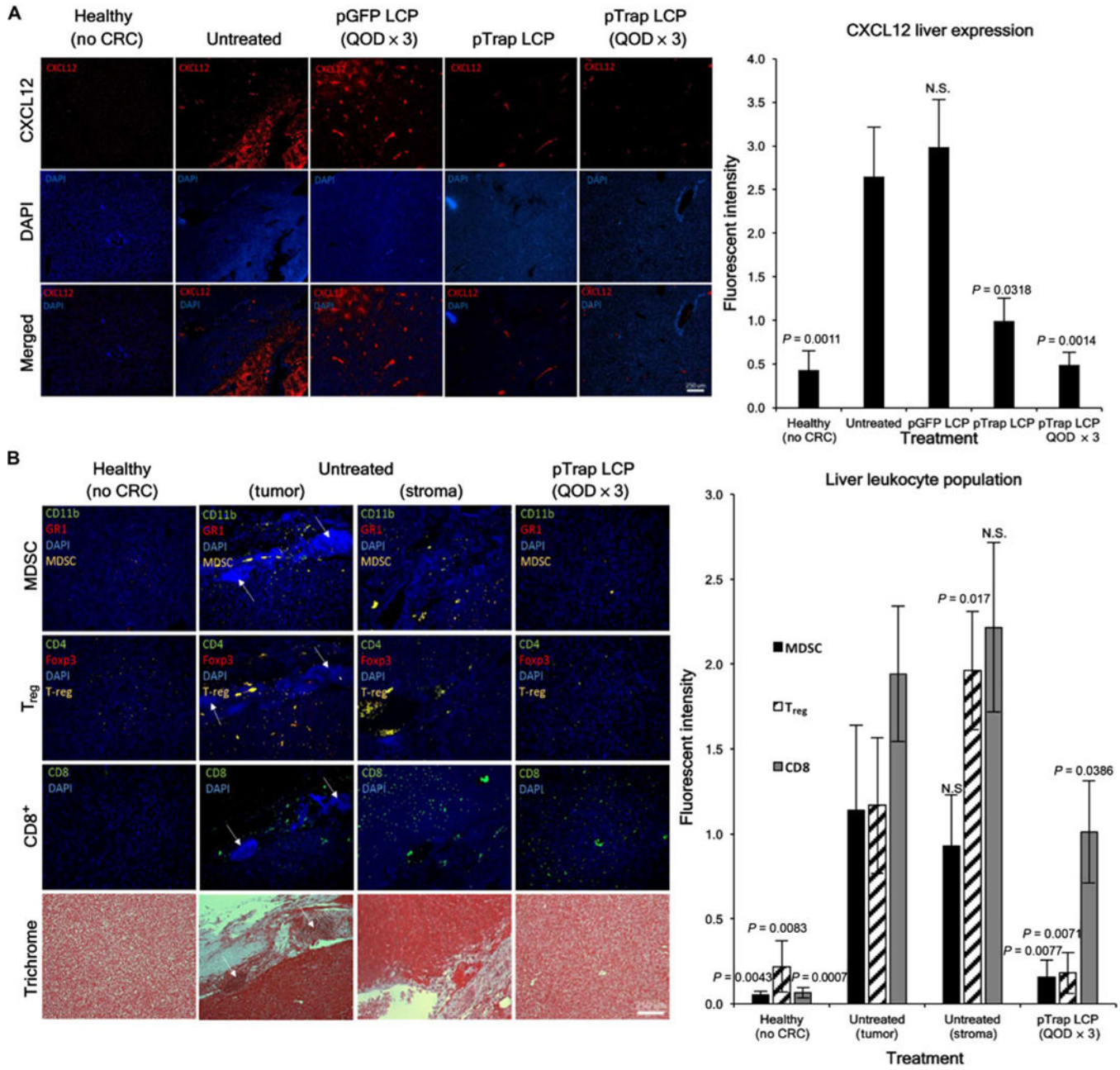

Fig. 3. Biological trapping of endogenous CXCL12 and immune cell recruitment

(**A**) Endogenous CXCL12 expression in paraffin-embedded sections of liver tissues from BALB/c mouse models of CRC sacrificed 10 days after the final treatment injection and control healthy livers [healthy (no CRC)]. Immunofluorescence stain for CXCL12 (red), along with DAPI nuclear stain (blue). Five groups were studied, including healthy (no CRC), untreated (PBS), pGFP LCP control [10 mg every other day (QOD) × 3], pTrap LCP (10 mg), and pTrap LCP (10 mg every other day × 3). All data are means ± SD, calculated from samples run in triplicate and reported as fluorescence intensity. The *P* values of individual groups compared to corresponding untreated control are displayed in graphs. (**B**) Additional sections were stained to determine the recruitment of immune cells to the liver, including

immunosuppressive anti-inflammatory MDSCs [CDllb$^+$ (green)/GR1$^+$ (red)] and T_{regs} [CD4$^+$ (green)/Foxp3$^+$ (red)] as well as the CD8$^+$ T cell population (green). Four groups were studied, including healthy (no CRC), untreated (tumor), untreated (stroma), and pTrap LCP (10 mg every other day × 3). Trichrome staining is also shown to distinguish normal and diseased liver. White arrows indicate metastatic lesions. All data are means ± SD, calculated from samples run in triplicate and reported as fluorescence intensity relative to untreated control. The *P* values of individual groups compared to corresponding untreated control are displayed in graphs. Scale bars, 250 μm.

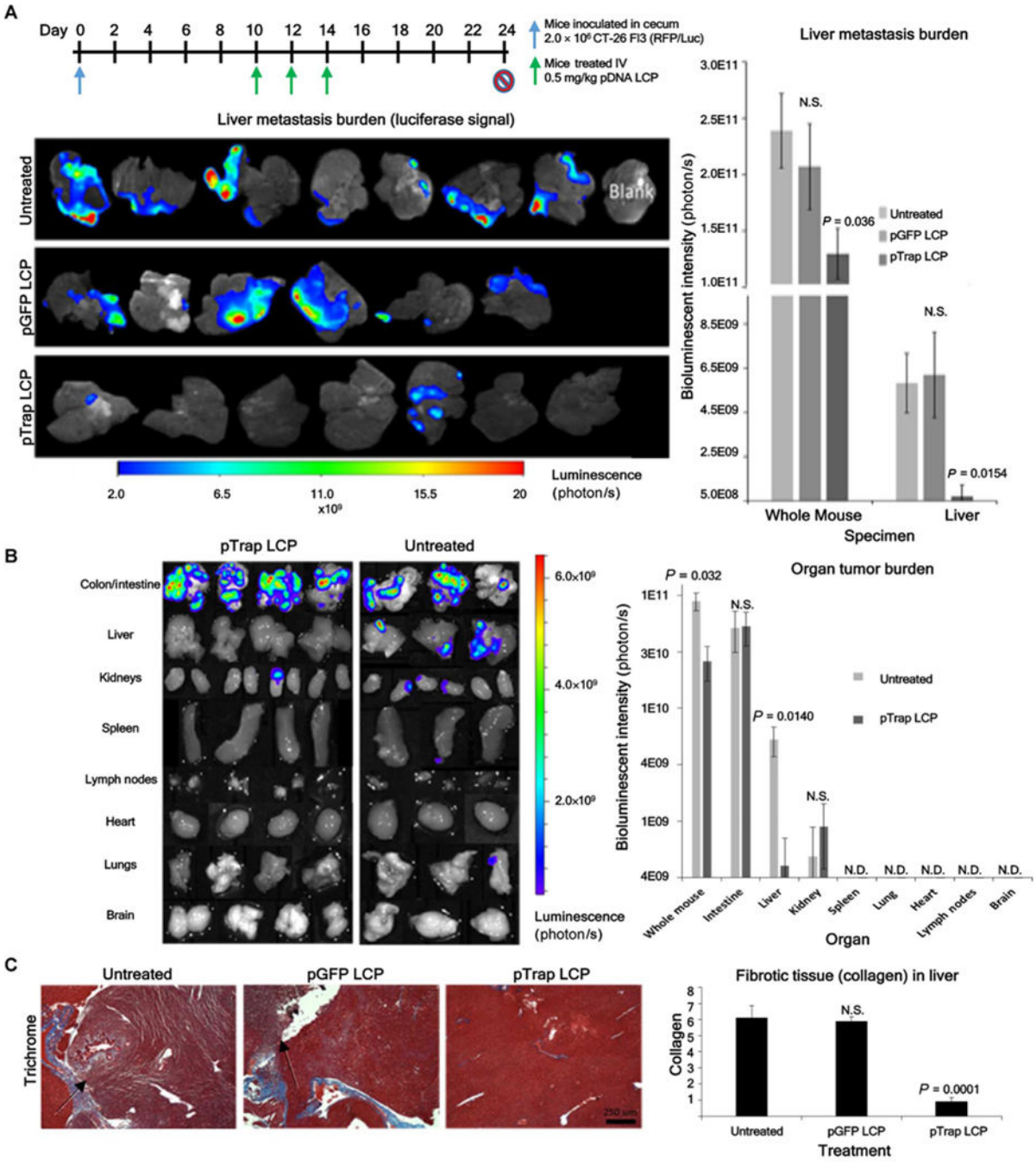

Fig. 4. Decreased incidence of liver metastasis after pTrap LCP treatment

(**A**) Mice were inoculated with 2 × 10^6 CT-26(FL3) RFP/Luc cells into the cecum wall. Treatment schedule is shown above. Treatment, 10 mg (0.5 mg/kg) of pDNA, was administered intravenously through the tail vein on days 10, 12, and 14. Groups included PBS (untreated; $n = 7$) and pGFP LCP (10 mg every other day × 3; $n = 6$), as well as pTrap LCP (10 mg every other day × 3; $n = 7$). Progression of overall tumor mass was followed by administration of 200 of ml luciferin (10 mg/ml) intraperitoneally. Luciferase bioluminescence imaging was recorded 10 min after administration of luciferin. Whole

mouse and liver tumor burden were recorded. All data are means ± SD and reported as bioluminescent intensity. The *P* values of individual groups compared to corresponding untreated control are displayed in graph. (**B**) Total organ tumor burden of untreated ($n = 3$) and therapeutic pTrap LCP ($n = 4$) groups. Quantification of tumor burden in organs was performed with IVIS/Kodak software. All data are means ± SD and reported as bioluminescent intensity. The *P* values of individual groups compared to corresponding untreated control are displayed in graph. (**C**) Paraffin-embedded liver sections were stained with trichrome. Large tumor burden (indicated by black arrows) and cirrhosis/fibrosis (blue stain, collagen) are clearly seen in the PBS (untreated) and pGFP LCP treatment groups. The pTrap LCP– treated livers have normal healthy liver morphology and no detectable metastatic burden. Scale bars, 250 μm. Collagen quantification in liver section was recorded. All data are means ± SD. The *P* values of individual groups compared to corresponding untreated control are displayed in graph.

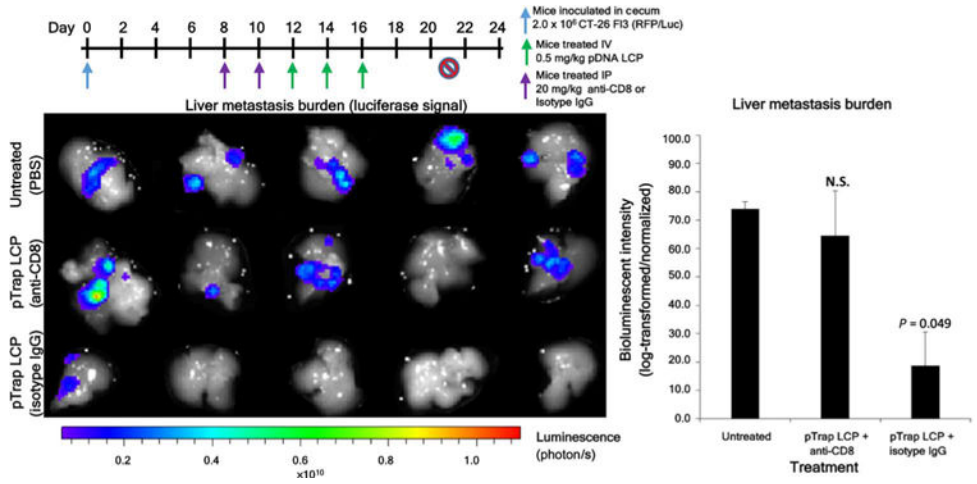

Fig. 5. Decreased incidence of liver metastasis and enhanced T cell killing after pTrap LCP therapy

Mice were inoculated with 2×10^6 CT-26(FL3) RFP/Luc cells into the cecum wall. Treatment, 10 mg (0.5 mg/kg) of pDNA, was administered intravenously through the tail vein on days 10, 12, and 14. Groups included PBS (untreated; $n = 5$) and pTrap LCP (10 mg every other day × 3; $n = 5$) with either anti-Lyt2.2 or isotype IgG control administrated on days 8 and 10 (400 mg, 20 mg/kg) intraperitoneally (IP). Inoculation and treatment schedule/dose and liver tumor mass on day 21 are shown above. Mice were administered 200 ml of luciferin (10 mg/ml) intraperitoneally. After 5 min, mice were euthanized, and livers were extracted, rinsed in PBS, and placed in a solution of luciferin (1 mg/ml). The bioluminescence images were recorded using IVIS Kinetic with Kodak camera. Quantification of tumor burden in the liver was performed with IVIS/Kodak software. Data were expressed as log-transformed mean, normalized ± SE. The *P* values of individual groups compared to corresponding untreated control are displayed in graph.

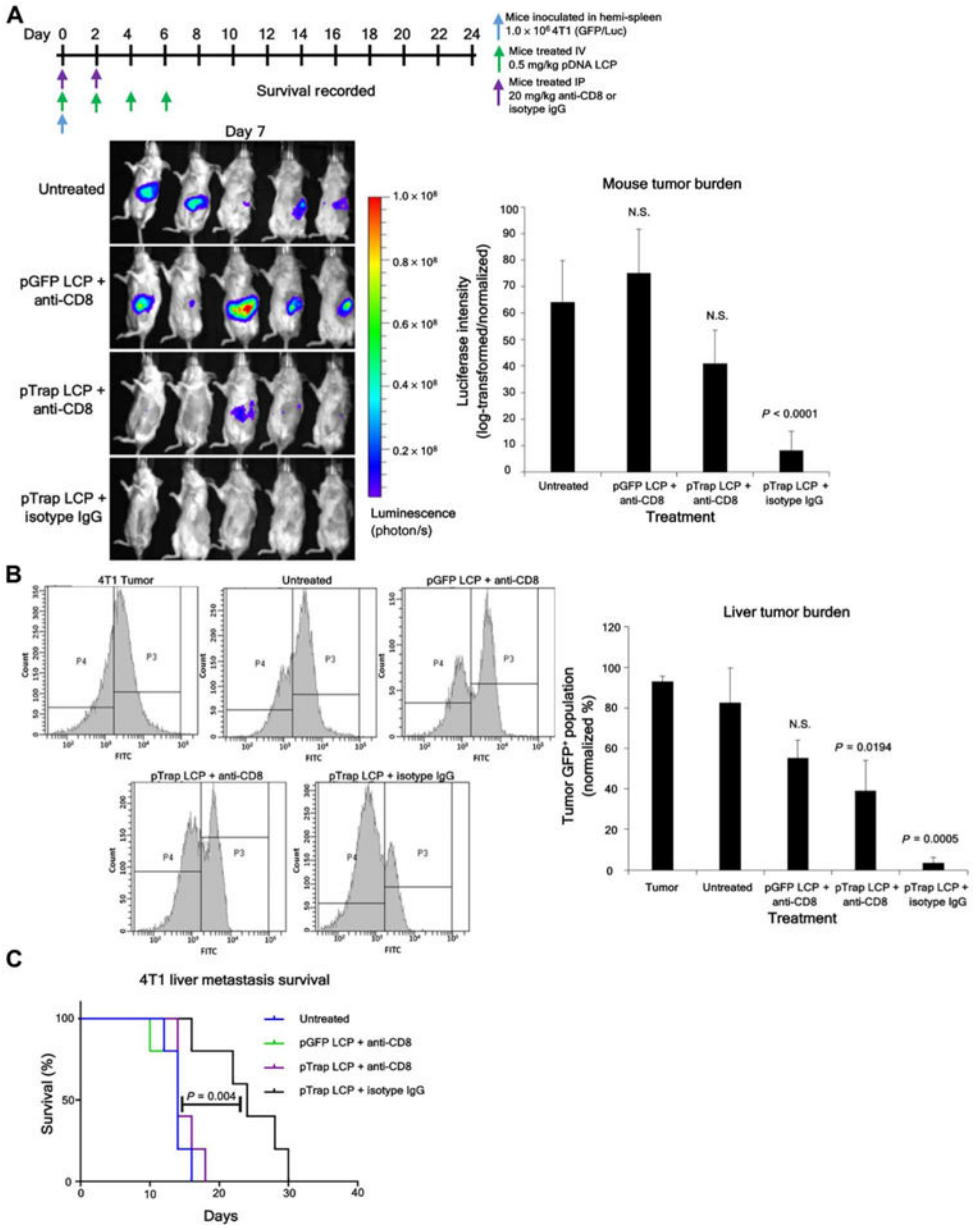

Fig. 6. Decreased incidence of 4T1 liver metastasis and increased survival after pTrap LCP treatment

(**A**) Inoculation and treatment schedule and doses, as well as bioluminescent signal detection and tumor burden quantification 7 days after inoculation. Treatment groups included PBS (untreated; $n = 5$), pGFP LCP/anti-CD8 ($n = 5$), pTrap LCP/anti-CD8 ($n = 5$), and pTrap LCP/isotype IgG ($n = 5$). Data were expressed as log-transformed mean, normalized ± SE. The P values of individual groups compared to corresponding untreated control are displayed in graph. (**B**) Flow cytometry analysis of tumor burden and quantification on day 10 ($n = 3$ per group). Gating consists of GFP^+ tumor cells (P3) versus non-GFP^+ cells (P4). Data were expressed as mean, normalized ± SD. The P values of individual groups compared to corresponding untreated control are displayed in graph. FITC, fluorescein isothiocyanate. (**C**) Kaplan-Meier survival curve including all four treatment groups ($n = 5$

per group). Survival was determined by evaluating mouse weight, activity, and quality of life. The *P* values of individual groups compared to corresponding untreated control are displayed in graph.

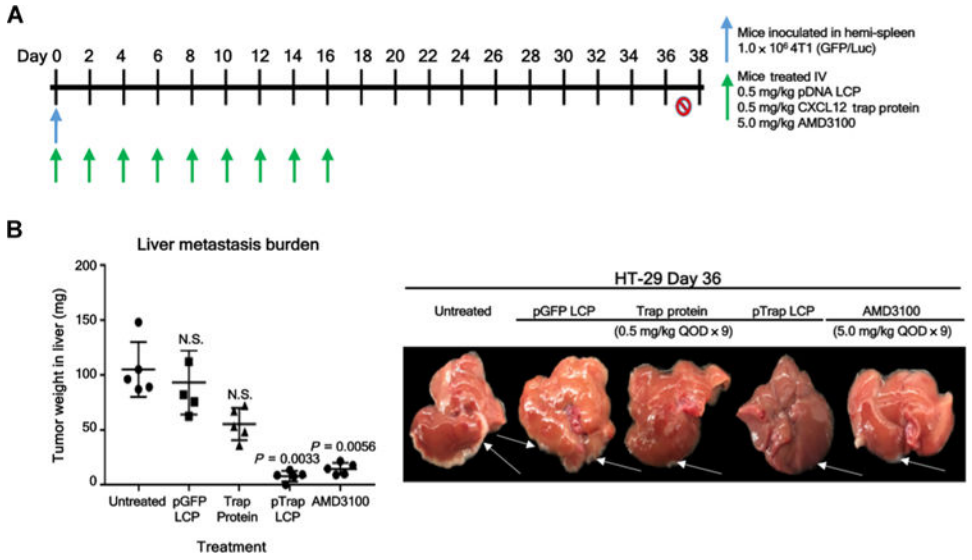

Fig. 7. Comparison of therapeutic strategies for reducing incidence of CRC (HT-29) liver metastasis

(**A**) The timeline at the top shows the inoculation and treatment schedule and dosing for the HT-29. Treatments were administered intravenously through the tail vein every other day on days 0 to 16. Treatment groups included PBS (untreated; $n = 5$), pGFP LCP [10 mg (0.5 mg/kg) of pDNA; $n = 5$], pTrap LCP [10 mg (0.5 mg/kg) of pDNA; $n = 5$], free CXCL12 trap protein [10 mg (0.5 mg/kg) of protein; $n = 5$], and AMD3100 (100 mg, 5.0 mg/kg; $n = 5$). (**B**) Tumor burden analysis and quantification on day 36 ($n = 5$ per group). Liver metastasis burden was quantified by resection and weighing of tumor nodules (in mg). The image shows a representative liver from each treatment group with metastatic burden shown, and white arrows indicate metastatic lesions. Survival was determined by evaluating mouse weight, activity, and quality of life. Data were expressed as individual data points with means ± SD. The P values of individual groups compared to corresponding untreated control are displayed in graph.

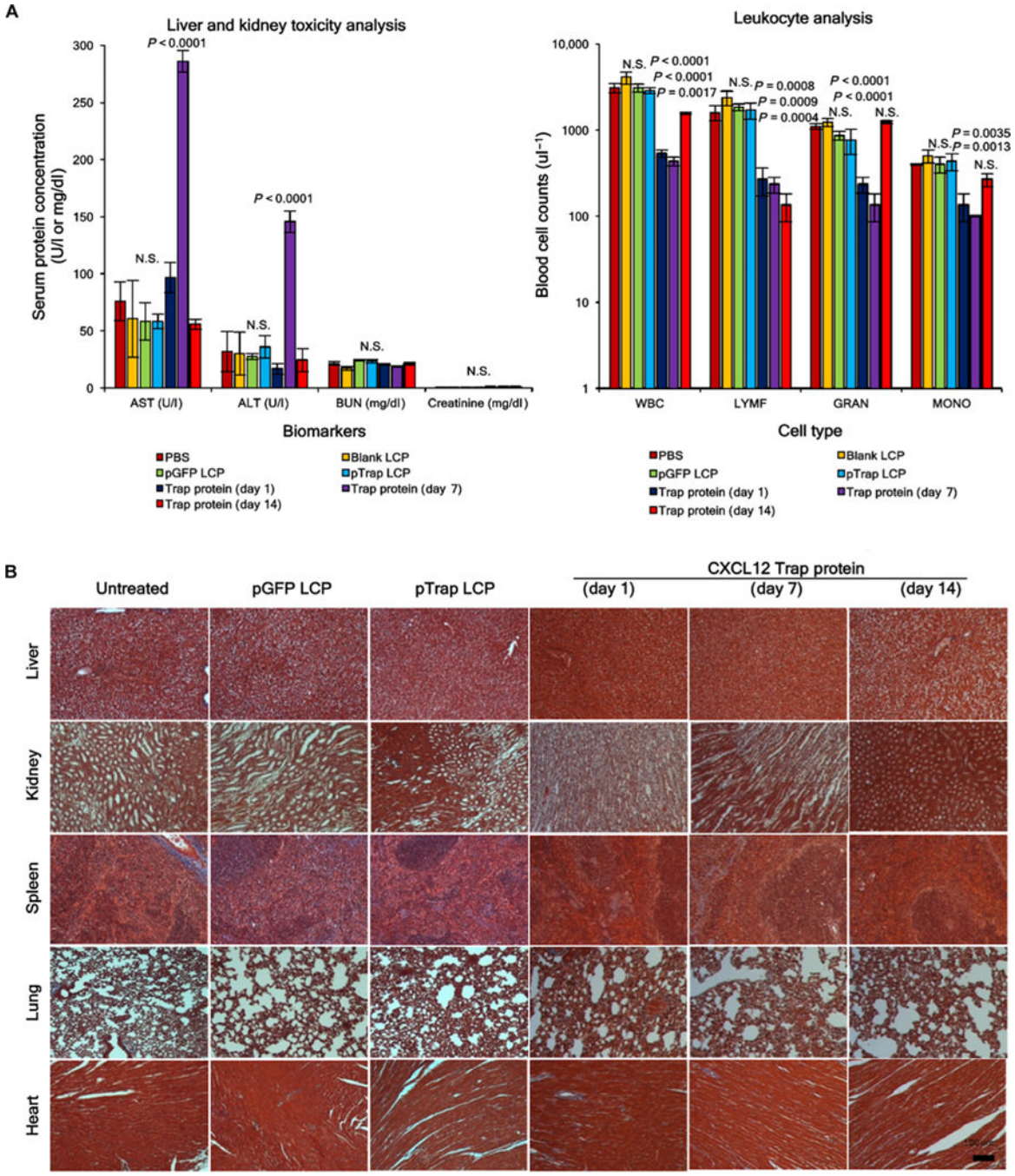

Fig. 8. Toxicological analysis

(**A**) ALT, AST, creatinine, and BUN measurements and blood leukocyte cell counts 24 hours after the final treatment with PBS (untreated), 10 mg of pGFP LCP (every other day × 3), 10 mg of pTrap LCP (every other day × 3), or 20 mg of free CXCL12 trap protein (every other day × 3), in which mice were sacrificed on days 1, 7, and 14 after the final administration. All data are means ± SD from samples run in triplicate. The *P* values of individual groups compared to corresponding untreated control are displayed in graph. (**B**) Trichrome histology sections of different organs 24 hours after the final treatment with PBS (untreated),

10 mg of pGFP LCP (every other day × 3), 10 mg of pTrap LCP (every other day × 3), or 20 mg of free CXCL12 trap protein (every other day × 3), in which mice were sacrificed on days 1, 7, and 14 after the final administration. All trichrome histology sections show no toxicity in any major organ including heart, lung, spleen, kidney, and liver. Scale bar, 100 μm.